Bona-Massó slices of Reissner-Nordström spacetimes

Sean E. Li[®], ^{1,*} Thomas W. Baumgarte[®], ^{1,†} Kenneth A. Dennison[®], ^{1,‡} and H. P. de Oliveira^{1,2,§}

¹Department of Physics and Astronomy, Bowdoin College, Brunswick, Maine 04011, USA

²Departamento de Física Teórica, Instituto de Física A. D. Tavares, Universidade do Estado do Rio de Janeiro, R. São Francisco Xavier, 524, 20550-013 Rio de Janeiro, Brazil

(Received 25 July 2022; accepted 14 November 2022; published 29 November 2022)

Motivated by recent numerical relativity simulations of charged black holes and their interactions, we explore the properties of common slicing conditions in Reissner-Nordström spacetimes. Specifically, we consider different choices for the so-called Bona-Massó function and construct static and spherically symmetric slices of the Reissner-Nordström spacetime satisfying the corresponding slicing conditions. For some of these functions the construction is entirely analytical, while for others we use numerical root-finding to solve quartic equations. Our solutions are parametrized by the charge-to-mass ratio $\lambda = Q/M$ and approach a unique slice, independent of the Bona-Massó functions considered here, in the extremal limit $\lambda \to 1$.

DOI: 10.1103/PhysRevD.106.104059

I. INTRODUCTION

In many numerical relativity simulations, the time coordinate is specified by imposing a slicing condition for the lapse function α . A very common condition is the Bona-Massó slicing condition [1]

$$(\partial_t - \beta^i \partial_i)\alpha = -\alpha^2 f(\alpha) K, \tag{1}$$

where β^i is the shift vector, $f(\alpha)$ a yet-to-be-specified function of the lapse, and $K \equiv K_i^i$ the mean curvature, i.e., the trace of the extrinsic curvature. Choosing a Bona-Massó function $f(\alpha)$ identifies a specific slicing of the spacetime; for f=1, for example, (1) reduces to harmonic slicing. A very common choice is $f=2/\alpha$, which results in so-called "1 + log" slicing. Combined with a "Gamma-driver" condition for the shift [2–4], 1 + log slicing forms the so-called "moving-puncture" coordinates that have been used, for example, in numerous simulations of black-hole binaries (see, e.g., [5,6]).

Significant insight into the properties of $1 + \log$ slicing, and hence our understanding of the above simulations, resulted from analytical studies of $1 + \log$ slices of the Schwarzschild spacetime (e.g., [7–11]). In particular, these studies revealed the "trumpet geometry" of the resulting slices, which helped to explain their remarkable numerical properties.

In recent years, several authors have also considered black holes with charge, and have simulated their interaction in the framework of Einstein-Maxwell theory [12–22]. In part, these simulations are motivated by astrophysical considerations—for example, to explore whether current observations of gravitational-wave signals can be used to place bounds on the black-hole charge—and in part by the recognition that Einstein-Maxwell theory is a well-posed example of a tensor-vector theory, and may therefore serve as a stand-in for more exotic extensions of general relativity. Many of the above simulations also adopt $1 + \log$ slicing, raising the question of whether its desirable properties for uncharged black holes also exist for charged black holes.

Motivated by these considerations we generalize in this paper previous work on Bona-Massó slices of Schwarzschild spacetimes to their charged counterparts, namely Reissner-Nordström (RN) spacetimes. Specifically, we follow [23] and consider a number of different families of Bona-Massó functions $f(\alpha)$, but apply these to charged, rather than uncharged, static black holes. We outline our mathematical approach in Sec. II, consider extremal black holes in Sec. III, discuss results for specific choices of the Bona-Massó function in Sec. IV, and briefly summarize in Sec. V.

Throughout this paper we use geometrized units with G = c = 1 and adopt the convention that indices a, b, c, \ldots represent spacetime indices while i, j, k, \ldots denote spatial indices.

II. BASIC EQUATIONS

Most of this section is a direct extension of previous work on $1 + \log$ slices of Schwarzschild spacetimes,

^{*}sli@bowdoin.edu

tbaumgar@bowdoin.edu

[‡]kdenniso@bowdoin.edu

[§]henrique.oliveira@uerj.br

e.g., [7,10,11]. We generalize those previous treatments by considering different families of Bona-Massó functions (see also [23]) and by applying these to Reissner-Nordström spacetimes.

A. Transformation to Bona-Massó slices

The line element for a nonrotating, charged black hole can be written as

$$ds^{2} = -f_{0}dt^{2} + f_{0}^{-1}dR^{2} + R^{2}d\Omega^{2},$$
 (2)

where we have defined

$$f_0 \equiv 1 - \frac{2M}{R} + \frac{Q^2}{R^2} \tag{3}$$

[not to be confused with the Bona-Massó function $f(\alpha)$ defined in Eq. (1)]. In the above equations, R is the areal radius, M the black-hole mass, and Q the black-hole charge. We also note that the two horizons of an RN spacetime are located at the roots of the function $f_0 = f_0(R)$, i.e., at

$$R_{+} = M \pm \sqrt{M^2 - Q^2}. (4)$$

We now transform to new spatial slices using a height function approach (see, e.g., Sec. IV. 2 in [24] for a textbook treatment), i.e., we write a new time coordinate \bar{t} as

$$\bar{t} = t + h(R). \tag{5}$$

By allowing the height function h = h(R) to depend on radius only, we restrict our focus to time-independent and spherically symmetric slices. Inserting (5) into the line element (2) then yields¹

$$ds^2 = -f_0 d\bar{t}^2 + 2f_0 h' d\bar{t} dR + (f_0^{-1} - f_0 h'^2) dR^2 + R^2 d\Omega^2, \eqno(6)$$

where the prime denotes differentiation with respect to R, $h' \equiv dh/dR$. We compare (6) with the general 3 + 1 form of the spacetime metric,

$$ds^{2} = -\alpha^{2}d\overline{t}^{2} + \gamma_{ij}(dx^{i} + \beta^{i}d\overline{t})(dx^{j} + \beta^{j}d\overline{t}), \quad (7)$$

to identify the RR-component of the spatial metric

$$\gamma_{RR} = f_0^{-1} - f_0 h^2, \tag{8}$$

the R-component of the shift vector

$$\beta^{R} = \frac{f_0 h'}{\gamma_{RR}} = \frac{f_0^2 h'}{1 - f_0^2 h'^2},\tag{9}$$

and the square of the lapse

$$\alpha^2 = f_0 + \gamma_{RR}(\beta^R)^2 = \frac{f_0}{1 - f_0^2 h'^2}.$$
 (10)

We note that α does not necessarily vanish at a root of f_0 , i.e., on the black-hole horizons, since h' may diverge there. Using (10) we may also rewrite the shift (9) as

$$\beta^R = \alpha \sqrt{\alpha^2 - f_0} = \alpha^2 |f_0 h'|, \tag{11}$$

where we have taken a positive root. We compute the mean curvature from

$$K = -\nabla_a n^a = -\frac{1}{\sqrt{|g|}} \partial_a \left(\sqrt{|g|} n^a \right), \tag{12}$$

where $g = -R^4 \sin^2 \theta$ is the determinant of the metric, and n^a the future-oriented normal of the hypersurface

$$n^a = \alpha^{-1}(1, -\beta^i). \tag{13}$$

For static and spherically symmetric slices, (12) becomes

$$K = \frac{1}{R^2} \frac{d}{dR} \left(R^2 \frac{\beta^R}{\alpha} \right) = \frac{2}{R} \frac{\beta^R}{\alpha} + \frac{(\beta^R)'}{\alpha} - \frac{\beta^R}{\alpha^2} \alpha' \quad (14)$$

and the Bona-Massó condition (1) reduces to

$$\beta^R \alpha' = \alpha^2 f(\alpha) K. \tag{15}$$

Substituting (14) into (15) then yields

$$\frac{d\alpha}{\alpha f(\alpha)} + \frac{d\alpha}{\alpha} = \frac{2dR}{R} + \frac{d\beta^R}{\beta^R},\tag{16}$$

which, using (11), we may integrate to obtain

$$\alpha^{2} = 1 - \frac{2M}{R} + \frac{Q^{2}}{R^{2}} + \frac{Ce^{2I(\alpha)}}{R^{4}}$$

$$= f_{0}(R) + \frac{Ce^{2I(\alpha)}}{R^{4}}.$$
(17)

In (17) we defined the integral

$$I(\alpha) \equiv \int_0^\alpha \frac{d\tilde{\alpha}}{\tilde{\alpha}f(\tilde{\alpha})},\tag{18}$$

and C is an undetermined constant of integration with units of M^4 . We note that the above expressions differ from their

¹See also [25,26], who adopted the height-function approach to construct maximal slices in nonextremal RN spacetimes, and [27], who constructed hyperboloidal slices of RN spacetimes using this approach.

counterparts for uncharged black holes only by the appearance of the term Q^2/R^2 in Eq. (17).

B. Regularity condition

We will be interested in regular slices that penetrate the outer horizon R_+ [see (4)], meaning that the lapse α should connect $\alpha=1$ in the asymptotic region $R\to\infty$ with a root $\alpha=0$ at a radius $R_0\le R_+$. If such a slice penetrated the inner horizon also we would have $f_0(R_0)>0$, in which case we could evaluate (17) at R_0 to find C<0. At either one of the horizons, however, (17) would then yield $\alpha^2<0$, which does not have a real solution. We therefore conclude that regular slices can penetrate the outer horizon only; those that do penetrate the outer horizon then have $R_- \le R_0 \le R_+$ with $f_0(R_0) \le 0$ and hence $C \ge 0$. As we observed below Eq. (10), the derivative of the height function h' will necessarily diverge at R_+ for such a slice.

For general values of the constant C in Eq. (17) the resulting lapse α will *not* connect a root at R_0 with the asymptotic region; instead, there may be regions at radii $R > R_0$ for which (17) does not yield real values of α at all. The regular slices that we are interested in therefore exist for special values of C only. In order to identify these values of C we follow [8,10] and consider an equation for the derivative of the lapse. Inserting (11) into both (14) and (15) we obtain

$$\alpha' = \frac{\alpha f(\alpha)}{M\hat{R}} \frac{2 - 3/\hat{R} + \lambda^2/\hat{R}^2 - 2\alpha^2}{1 - 2/\hat{R} + \lambda^2/\hat{R}^2 + \alpha^2 f(\alpha) - \alpha^2}$$

$$= \frac{\alpha f(\alpha)}{M\hat{R}} \frac{2 - 3/\hat{R} + \lambda^2/\hat{R}^2 - 2\alpha^2}{f_0(R) + \alpha^2 (f(\alpha) - 1)},$$
(19)

where we have introduced a dimensionless areal radius $\hat{R} \equiv R/M$ and the dimensionless charge-to-mass ratio $\lambda \equiv Q/M$. We now observe that the denominator on the right-hand side may have a root for $R > R_0$; if so, α' can remain regular at that root of the denominator only if the numerator has a simultaneous root. The radius and lapse at such a critical point (denoted by \hat{R}_c and α_c) must therefore satisfy the two equations²

$$2 - \frac{3}{\hat{R}_c} + \frac{\lambda^2}{\hat{R}_c^2} - 2\alpha_c^2 = 0 \quad \text{and}$$
 (20a)

$$1 - \frac{2}{\hat{R}_c} + \frac{\lambda^2}{\hat{R}_c^2} + \alpha_c^2 f(\alpha_c) - \alpha_c^2 = 0,$$
 (20b)

where we have assumed that the root of the denominator of (19) results from a vanishing of the denominator of the second fraction in (19), rather than the first.

We can eliminate λ from Eqs. (20) to obtain one equation for \hat{R}_c and α_c alone,

$$\hat{R}_c = \frac{1}{1 - \alpha_c^2 f(\alpha_c) - \alpha_c^2}.$$
 (21)

We then reinsert (21) into (20a) and, depending on the specific choice of $f(\alpha)$, find α_c either by numerical root-finding for a given λ or by solving for α_c analytically. Given α_c we then find \hat{R}_c from (21), and finally insert both into (17) to obtain the constant C.

The above procedure works as long as $\alpha f(\alpha)$ in the first term on the right-hand side of (19) remains finite as $\alpha \to 0$. This is the case for most Bona-Massó functions considered in this paper, but not for the shock-avoiding slices with $f(\alpha) = 1 + \kappa/\alpha^2$ (see [28]). For the latter, the (outer-most) root of the denominator of Eq. (19) occurs for $\alpha = 0$ rather than a root of (20b), provided κ satisfies condition (52). Inserting $\alpha_c = 0$ into (20a) then yields the critical radius \hat{R}_c (see also Sec. IV C 1 below).

C. The root of the lapse

For a given $f(\alpha)$ whose integral $I(\alpha)$ is known, evaluating (17) at the critical point, for known values of \hat{R}_c and α_c , allows computing the constant of integration C. From there, we compute the root \hat{R}_0 of the lapse by setting $\alpha=0$ in (17). For some choices of the Bona-Massó function $f(\alpha)$ we can solve the resulting quartic equation for \hat{R}_0 analytically, while for others we use numerical root-finding.

As the next step we compute the dimensionless derivative of the lapse evaluated at its root,

$$\hat{a}_1 \equiv M\alpha'(\hat{R}_0). \tag{22}$$

In most cases this is done via implicit differentiation of (17), except for the fully shock-avoiding slicing condition of Sec. IV C, for which it is more convenient to take the limit $\hat{R} \rightarrow \hat{R}_0$ of Eq. (19). In order to choose valid roots \hat{R}_0 among the real solutions to the above quartic equation we check that $\hat{a}_1 \ge 0$ so that the lapse stays non-negative near the root.

²Assuming that $\alpha^2(f(\alpha)-1)$ vanishes for $\alpha=0$, and that $f(\alpha)>1$ for all α , horizon-penetrating slices necessarily go through a critical point at a point R_c such that $R_0 \leq R_c \leq R_+$. This is because $f_0(R)$ has a root at R_+ , while $-\alpha^2(f(\alpha)-1)$ has a root at R_0 ; both are nonpositive between these two points, and intersect so that the denominator of the second term of (19) vanishes. The assumption $f(\alpha)>1$ for all α holds for most Bona-Massó functions considered in this paper, but not for the analytical trumpet slices of Sec. IV B. For the latter it is possible to construct slices that avoid a critical point altogether, but we will instead focus on slices that pass through a critical point in this paper.

D. Transformation to isotropic coordinates

Finally, we transform to isotropic coordinates with radial coordinate r. To do so, we compare the spatial part of the line element (6),

$$dl^2 = \alpha^{-2}dR^2 + R^2d\Omega^2, \tag{23}$$

with the spatial line element in isotropic coordinates,

$$dl^{2} = \psi^{4}(dr^{2} + r^{2}d\Omega^{2}), \tag{24}$$

where ψ is a conformal factor, which yields the system

$$\alpha^{-1}dR = \psi^2 dr \quad \text{and} \tag{25a}$$

$$R = \psi^2 r. \tag{25b}$$

Together, Eqs. (25) yield

$$\frac{dr}{r} = \frac{dR}{R\alpha} = \frac{dR/d\alpha}{R} \frac{d\alpha}{\alpha},$$
 (26)

which we may integrate to obtain

$$r = \exp \int \frac{dR/d\alpha}{R} \frac{d\alpha}{\alpha}.$$
 (27)

Making the leading-order approximation $dR/d\alpha \simeq 1/a_1$ and $R \simeq R_0$, we further integrate (27) to find

$$\alpha \propto r^{1/\gamma} \ (r \to 0),$$
 (28)

where we have adopted the notation of [11] in defining

$$\gamma \equiv \frac{1}{\hat{a}_1 \hat{R}_0}.\tag{29}$$

For general values of $R > R_0$ we integrate (27) following the prescription laid out in Eqs. (46), (47), and (67) of [11] in order to obtain the isotropic radius r as a function of the areal radius R. As a consistency check we verify that, in the vicinity of the root, the lapse behaves according to the power law (28) (see also Eq. (56) in [11]). Having obtained r, we can compute the conformal factor ψ from (25b) as

$$\psi = \sqrt{\frac{R}{r}},\tag{30}$$

where we see that near the root of the lapse, where R approaches R_0 , we have

$$\psi \propto r^{-1/2} \ (r \to 0) \tag{31}$$

as is characteristic for a trumpet geometry.

III. THE EXTREMAL LIMIT

Before discussing specific choices for the Bona-Massó function $f(\alpha)$ in Sec. IV we first consider extremal Reissner-Nordström black holes with Q=M, i.e., $\lambda=1$. For $\lambda=1$, Eq. (17) becomes

$$\alpha^2 = \left(\frac{\hat{R} - 1}{\hat{R}}\right)^2 + \frac{\hat{C}e^{2I(\alpha)}}{\hat{R}^4},\tag{32}$$

where we have defined the dimensionless constant of integration $\hat{C} = M^{-4}C$. Since the exponential term is always positive, solutions for the lapse must have $C \le 0$ in order to have a root in this case, independently of the choice of $f(\alpha)$.

As we discussed in Sec. II B, the procedure for finding the critical point depends on the behavior of $\alpha f(\alpha)$ as $\alpha \to 0$. If $\alpha f(\alpha)$ remains finite in this limit, we identify the critical point by finding simultaneous roots of Eqs. (20). In the extremal limit, we may then rewrite Eq. (20b) as

$$\left(1 - \frac{1}{\hat{R}_c}\right)^2 + \alpha_c^2(f(\alpha_c) - 1) = 0.$$
 (33)

Assuming $f(\alpha_c) > 1$, (33) implies that the only critical point for non-negative α_c occurs at $\hat{R}_c = 1$ with $\alpha_c = 0$ (for which (20a) features a root also). Inserting these values into (17) then yields C = 0 in the extremal limit.

For shock-avoiding slices with $f(\alpha) = 1 + \kappa/\alpha^2$, on the other hand, the critical point is given by $\alpha_c = 0$ and \hat{R}_c by a root of (20a). In the extremal limit, these two roots are $\hat{R}_0 = 1$ and $\hat{R}_0 = 1/2$. Only for the former, however, does \hat{a}_1 take a nonimaginary value, so that we obtain the exact same critical values as in the case above.

For all Bona-Massó functions $f(\alpha)$ considered here we therefore have $\hat{C}=0$ in the extremal limit, so that Eq. (17) yields

$$\alpha = \frac{\hat{R} - 1}{\hat{R}} \tag{34}$$

independently of $f(\alpha)$. Finally, we observe that we have $\hat{a}_1 = 1$ and hence $1/\gamma = 1$ in the extremal limit.

IV. RESULTS FOR SPECIFIC SLICES

In the following we consider four different families of Bona-Massó functions and explore the associated slicing conditions. For each one we compute values of the parameters \hat{R}_c , α_c , \hat{C} , \hat{R}_0 , and $1/\gamma$ for different values of $\lambda = Q/M$ (see Figs. 1 and 2). For each family we also compute profiles of the lapse³ as a function of the isotropic radius and show results for selected values of λ in Figs. 3, 4, 5, 6.

³The lapse α as a function of R can be found from Eq. (17) using root-finding; we found it helpful to adopt α_c as an initial guess.

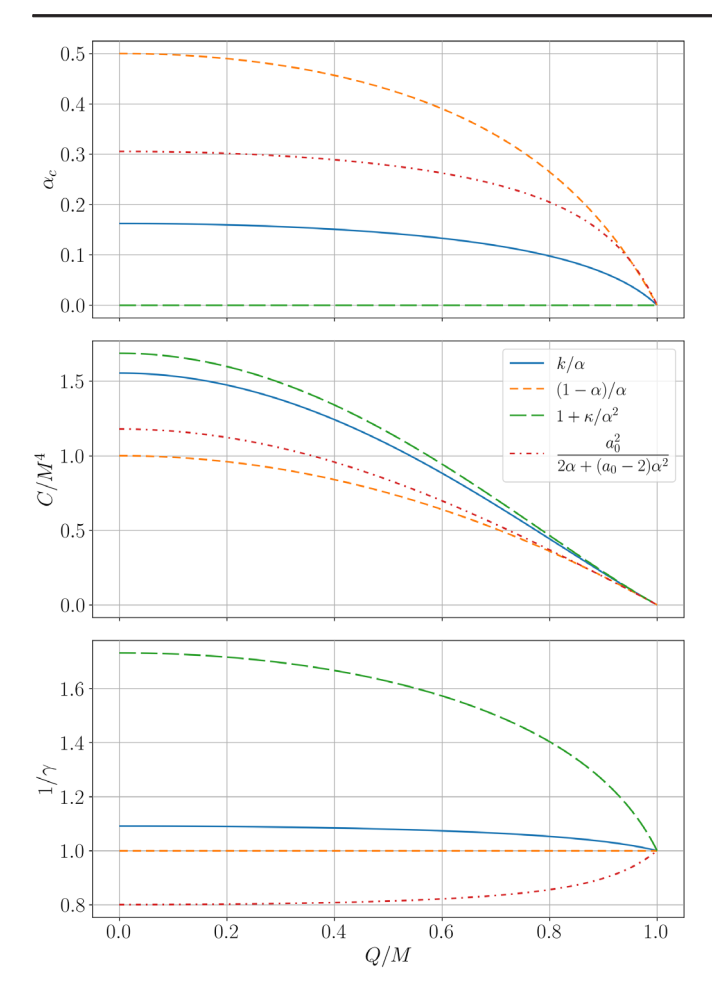


FIG. 1. The critical lapse α_c (top), constant of integration C (center), and exponent $1/\gamma$ (bottom) plotted against the charge-to-mass ratio λ (up to 0.999) on a shared horizontal axis for each of the slices given by $f(\alpha)$ that we consider. The solid (blue) line corresponds to $1 + \log$ slices (with k = 2), the short-dashed (orange) line to analytical trumpet slices, the long-dashed (green) line to fully gauge-shock-avoiding slices (with $\kappa = 1$), and the dash-dotted (red) line to zeroth-order gauge-shock-avoiding slices (with $a_0 = 4/3$). All slicing conditions yield the same critical values in the extremal limit $Q \to M$.

A. 1 + log slicing

We first consider Bona-Massó functions of the form

$$f(\alpha) = \frac{k}{\alpha}. (35)$$

Even though, strictly speaking, $1 + \log$ slicing corresponds to the case k = 2 only (see [1]), we refer to the entire family as " $1 + \log$ " slicing. For (35), the integral (18) can be evaluated to yield $I(\alpha) = \alpha/k$, so that (17) becomes

$$\alpha^2 = 1 - \frac{2}{\hat{R}} + \frac{\hat{\lambda}^2}{\hat{R}^2} + \frac{\hat{C}e^{2\alpha/k}}{\hat{R}^4}.$$
 (36)

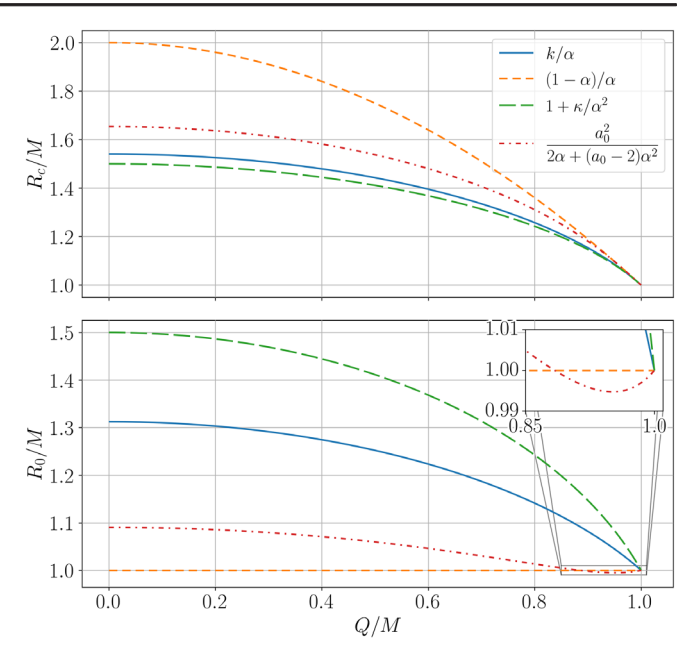


FIG. 2. The critical areal radius R_c (top) and the areal radius R_0 at which the lapse vanishes (bottom) versus λ for each $f(\alpha)$. The inset in the top-right corner of the bottom panel shows an expanded view of the bottom-right region, where the root of the lapse for zeroth-order shock-avoiding slices falls slightly below $\hat{R}_0 = 1$ near the extremal limit.

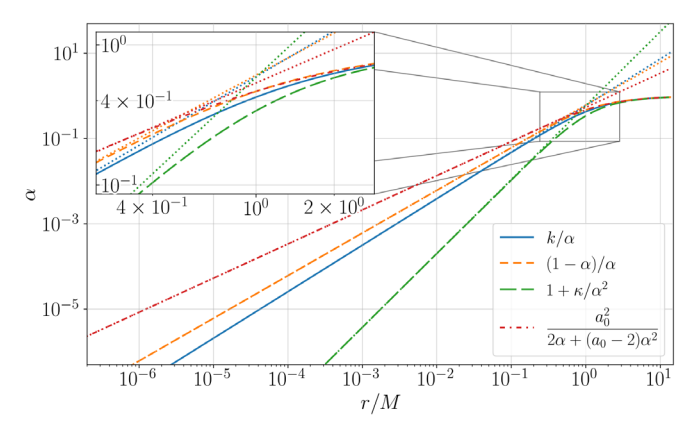


FIG. 3. Profiles of the lapse α as a function of isotropic radius r for each of the slices we consider (with k=2, $\kappa=1$, and $a_0=4/3$), with charge-to-mass ratio $\lambda=0$ (the Schwarzschild spacetime). The dotted lines represent the expected power-law behavior $\alpha \propto r^{1/\gamma}$ in the limit $r \to 0$. The inset in the top-left corner expands a crowded region of the plot where the lapse profiles depart from their small-radius power-law behavior.

Evaluating this either at the critical point (for α_c and \hat{R}_c) or at the root of the lapse (for $\alpha=0$ and \hat{R}_0) yields two different expressions for the constant of integration, namely

$$\hat{C} = \hat{R}_c^4 e^{-2\alpha_c/k} \left(\alpha_c^2 - 1 + \frac{2}{\hat{R}_c} - \frac{\lambda^2}{\hat{R}_c^2} \right)$$
 (37)

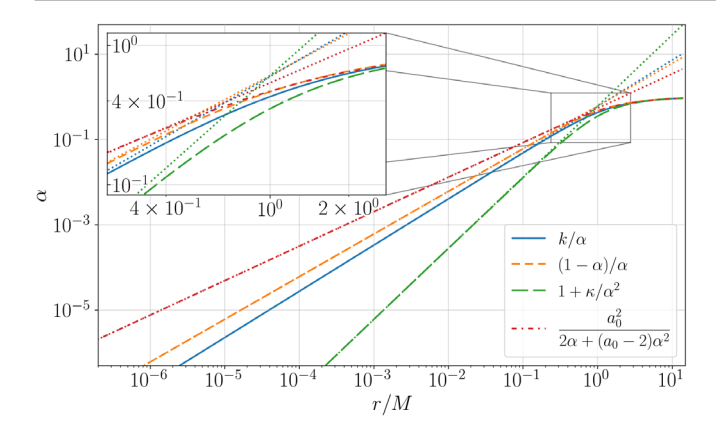


FIG. 4. Same as Fig. 3, but with $\lambda = 0.400$.

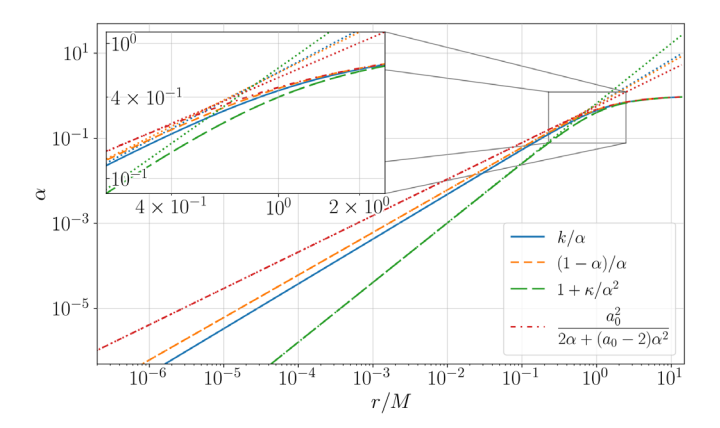


FIG. 5. Same as Fig. 3, but with $\lambda = 0.800$.

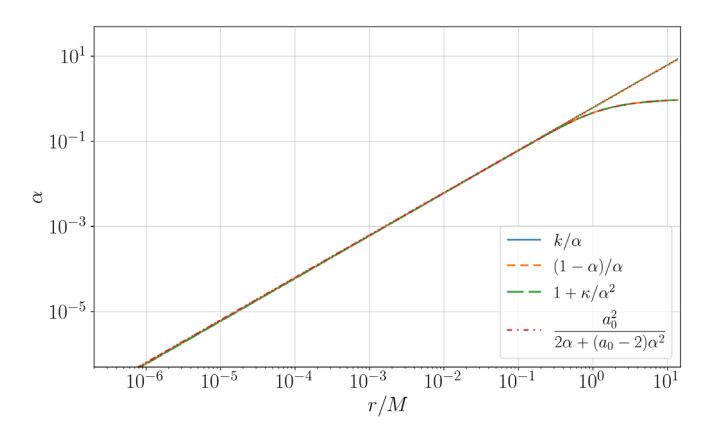


FIG. 6. Same as Fig. 3, but with $\lambda = 0.999$.

$$= -\hat{R}_0^4 + 2\hat{R}_0^3 - \lambda^2 \hat{R}_0^2. \tag{38}$$

Inserting (35) into (21) and then substituting (21) for \hat{R}_c in (20a), we obtain a quartic equation for α_c whose analytical solution is unwieldy. We thus use numerical root-finding to determine the critical point for these slices. The solution to (38) for \hat{R}_0 is similarly unwieldy, so we again use numerical root-finding to locate the root of the lapse.

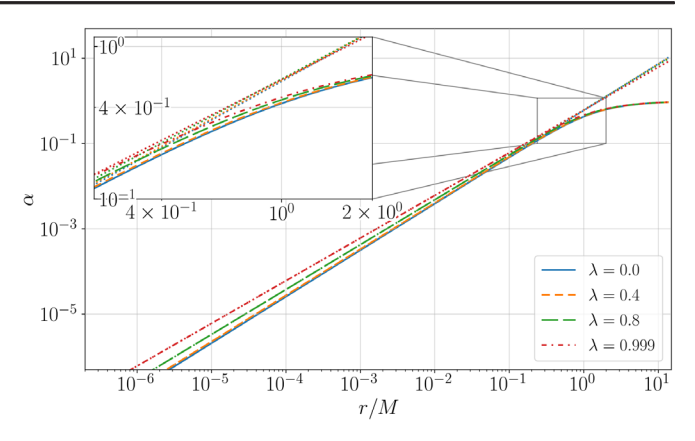


FIG. 7. The numerical profile of the lapse $\alpha(r)$ for $\lambda \in \{0, 0.4, 0.8, 0.999\}$ for $1 + \log$ slices with k = 2. See Fig. 3 for an explanation of the inset and dotted lines.

Implicit differentiation of (36) yields

$$\hat{a}_1 = \frac{-2\hat{R}_0^3 + 2\lambda^2 \hat{R}_0^2 + 4\hat{C}}{(2\hat{C}/k)\hat{R}_0},\tag{39}$$

from which we evaluate the exponent $1/\gamma = \hat{a}_1 \hat{R}_0$. We show graphs of all the above parameters, as a function of λ , in Figs. 1 and 2, together with the corresponding results for the other slicing conditions discussed in the following subsections.

Finally, we carry out the transformation from the areal radius R to isotropic radius r as discussed in Sec. II D, and show profiles of the lapse for $1 + \log$ slices for a few selected values of λ in Fig. 7.

B. Analytical trumpet slices

We next consider

$$f(\alpha) = \frac{1 - \alpha}{\alpha},\tag{40}$$

which, for uncharged black holes, results in the completely analytical trumpet slices of [29]. Inserting (40) into Eq. (20) yields the critical lapse

$$\alpha_c = \frac{1 - \lambda^2}{2 - \lambda^2},\tag{41}$$

together with the critical radius

$$\hat{R}_c = 2 - \lambda^2. \tag{42}$$

With $I(\alpha) = -\ln(1-\alpha)$, (17) becomes

$$\alpha^2 = 1 - \frac{2}{\hat{R}} + \frac{\lambda^2}{\hat{R}^2} + \frac{\hat{C}}{\hat{R}^4 (1 - \alpha)^2}.$$
 (43)

Substituting (41) and (42) into (43), we then obtain the constant of integration

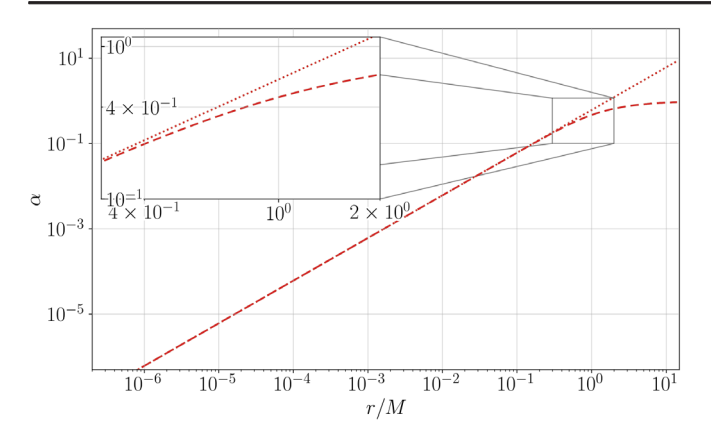


FIG. 8. The analytical profile of the lapse $\alpha(r)$ for analytical trumpet slices does not depend on the black-hole charge.

$$\hat{C} = 1 - \lambda^2. \tag{44}$$

Inserting the above into (43) and searching for roots of the lapse yields a quartic equation for \hat{R}_0 with two real solutions, one of which is $\hat{R}_0 = 1$. We compute

$$\hat{a}_1 = \frac{-\hat{R}_0^3 + \lambda^2 \hat{R}_0^2 + 2\hat{C}}{\hat{C}\hat{R}_0} \tag{45}$$

by implicit differentiation of (43) and find that $\hat{R}_0 = 1$ is the only root for which $\hat{a}_1 > 0$. In particular, for $\hat{R}_0 = 1$, we find $\hat{a}_1 = 1$, and hence $1/\gamma = 1$, independently of the charge-to-mass ratio λ .

Substituting (44) into (43), we find two real solutions for the lapse as a function of the areal radius. Only the solution

$$\alpha(R) = \frac{\hat{R} - 1}{\hat{R}},\tag{46}$$

however, which is identical to the extremal solution (34) but, remarkably, holds for all values of λ , satisfies $\alpha' > 0$ for all \hat{R} . We confirm that (46) agrees with the trumpet slices derived in [30] in the appropriate limit.

We take the solution for the lapse (46) and convert from areal radius R to isotropic radius r as explained in Sec. II D, and show our results for the lapse $\alpha(r)$ in Fig. 8.

C. Slices that avoid gauge shocks

1. Full gauge-shock avoidance

We next consider Bona-Massó functions of the form

$$f(\alpha) = 1 + \frac{\kappa}{\alpha^2} \tag{47}$$

with $\kappa > 0$, which Alcubierre [28] proposed as an alternative to $1 + \log$ slicing that helps avoid gauge-shocks, i.e., coordinate discontinuities that arise during evolution

(see also [31] for applications in simulations of critical collapse, and [32] for tests and calibrations).

With $f(\alpha)$ given by (47), Eq. (19) becomes

$$M\alpha' = \frac{\alpha^2 + \kappa}{\alpha \hat{R}} \frac{2 - 3/\hat{R} + \lambda^2/\hat{R}^2 - 2\alpha^2}{1 - 2/\hat{R} + \lambda^2/\hat{R}^2 + \kappa}.$$
 (48)

As we had discussed in Sec. II B, the denominator of the right-hand side now vanishes for $\alpha = 0$. For $\alpha = 0$, the numerator of (48), i.e., Eq. (20a), has a root for

$$\hat{R}_c = \frac{3 + \sqrt{9 - 8\lambda^2}}{4} \tag{49}$$

(where we have chosen the "outermost" solution to a quadratic equation for \hat{R}_c).

It is possible, of course, that the denominator of the second factor in (48) has a root for a radius larger than \hat{R}_c as determined in (49). This root occurs at a radius

$$\hat{R}_c^{\text{alt}} = \frac{1 + \sqrt{1 - \lambda^2 (1 + \kappa)}}{1 + \kappa}$$
 (50)

(which we note exists only for $\kappa \le 1/\lambda^2 - 1$). Substituting (50) into (20a) we find the corresponding critical lapse

$$\alpha_c^{\text{alt}} = \left(\frac{-1 + \sqrt{1 - \lambda^2(\kappa + 1)} - \lambda^2(\kappa - 1)}{2}\right)^{1/2} \frac{1}{\lambda}.$$
 (51)

We observe that for

$$\kappa > 1 - \frac{3 - \sqrt{9 - 8\lambda^2}}{2\lambda^2} \tag{52}$$

no real solutions for $\alpha_c^{\rm alt}$ exist, and conclude that, in this case, the critical radius \hat{R}_c is given by (49) with $\alpha_c = 0$. In the limit $\lambda \to 0$ condition (52) reduces to $\kappa > 1/3$, in agreement with [23].

From here we assume that condition (52) holds, and hence adopt the value (49) for \hat{R}_c together with $\alpha_c = 0$. As in [23] we may integrate (18) to obtain

$$I(\alpha) = \frac{1}{2} \ln \left(\frac{\alpha^2 + \kappa}{\kappa} \right), \tag{53}$$

so that (17) becomes

$$\alpha^{2} = 1 - \frac{2}{\hat{R}} + \frac{\lambda^{2}}{\hat{R}^{2}} + \frac{\alpha^{2} + \kappa}{\kappa} \frac{\hat{C}}{\hat{R}^{4}}.$$
 (54)

Solving for the constant of integration \hat{C} we obtain

$$\hat{C} = -\hat{R}_c^4 \left(1 - \frac{2}{\hat{R}_c} + \frac{\lambda^2}{\hat{R}_c^2} \right),\tag{55}$$

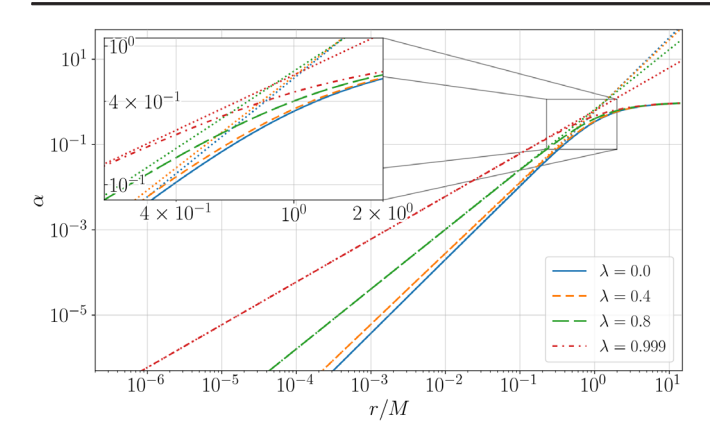


FIG. 9. The analytical profile of the lapse $\alpha(r)$ for $\lambda \in \{0, 0.4, 0.8, 0.999\}$ for fully gauge-shock-avoiding slices with $\kappa = 1$.

and substituting (49) for \hat{R}_c yields

$$\hat{C} = \frac{27}{32} + \frac{1}{32} (9 - 8\lambda^2)^{3/2} - \frac{9\lambda^2}{8} + \frac{\lambda^4}{4}.$$
 (56)

For $\lambda = 0$, we recover $\hat{C} = 3^3/2^4$ as found by [23].

To evaluate \hat{a}_1 , we apply L'Hôpital's rule to (48) and impose $M\alpha' \to \hat{a}_1$ as $\alpha \to 0$ to find

$$\hat{a}_1 = \sqrt{\frac{\kappa(4\hat{R}_0 - 3)}{(1 + \kappa)\hat{R}_0^3 - 2\hat{R}_0^2 + \lambda^2\hat{R}_0}}.$$
 (57)

Using (49) again we then have

$$\frac{1}{\gamma} = \left(\frac{18\kappa + 6\kappa\sqrt{9 - 8\lambda^2} - 16\lambda^2\kappa}{9\kappa + (3\kappa - 1)\sqrt{9 - 8\lambda^2} + 4\lambda^2(1 - \kappa) - 3}\right)^{1/2} \tag{58}$$

and verify that we recover

$$\frac{1}{\gamma} = \sqrt{\frac{6\kappa}{3\kappa - 1}}\tag{59}$$

for $\lambda = 0$ as in [23]. In the extremal limit $\lambda = 1$, (58) reduces to $1/\gamma = 1$ independently of κ , as expected from our discussion in Sec. III.

We obtain an analytical expression for the lapse as a function of areal radius by inserting (56) into (54),

$$\alpha(R) = \left(\frac{32\hat{R}^4 - 64\hat{R}^3 + 32\lambda^2\hat{R}^2 + 27 + (9 - 8\lambda^2)^{3/2} - 36\lambda^2 + 8\lambda^4}{32\kappa\hat{R}^4 - 27 - (9 - 8\lambda^2)^{3/2} + 36\lambda^2 - 8\lambda^4}\right)^{1/2}\sqrt{\kappa}.$$
(60)

We use the above solution to transform from areal radius R to isotropic radius r as described in Sec. II D, and show results for the lapse $\alpha(r)$ in Fig. 9.

2. Shock-avoidance to leading order

The fully shock-avoiding slicing condition given by (47) has the unusual property that it allows the lapse function to become negative during a numerical evolution (see [28,32,33]). Following [33] we therefore consider a leading-order shock-avoiding condition

$$f(\alpha) = \frac{a_0^2}{2\alpha + (a_0 - 2)\alpha^2} \tag{61}$$

(see, e.g., [34,35] for numerical applications). We note that $1 + \log$ slicing (35) with k = 2 is a member of this family for $a_0 = 2$.

As in [23] we can find the integral (17) analytically,

$$I(\alpha) = \frac{\alpha}{2a_0^2} (4 - (a_0 - 2)\alpha),\tag{62}$$

and may therefore evaluate the derivative of the lapse at its root to find

$$\hat{a}_1 = a_0^2 \frac{-2\hat{R}_0^3 + 2\lambda^2 \hat{R}_0^2 + 4\hat{C}}{4\hat{C}\hat{R}_0}.$$
 (63)

Expressions for the critical point (α_c, \hat{R}_c) , the constant \hat{C} , and the root of the lapse \hat{R}_0 , however, are more complicated, and we therefore find these quantities numerically (see Figs. 1 and 2).

Using these values, we compute the lapse by applying numerical root-finding to (17), then transform from areal to isotropic radius as in Sec. II D, and plot the lapse profile $\alpha(r(R))$ for a few chosen λ in Fig. 10.

V. SUMMARY

The $1 + \log$ slicing condition has been extremely successful in many numerical relativity simulations, including simulations of black holes and their binaries. Our understanding and interpretation of these simulations have greatly benefited from analytical studies that applied this and other slicing conditions to single, static, and spherically symmetric black holes, i.e., the Schwarzschild spacetime (e.g., [8–11,23]).

Motivated by recent simulations of charged black holes and their interactions we generalize some of the above treatments by applying them to the charged counterpart of Schwarzschild black holes, namely Reissner-Nordström

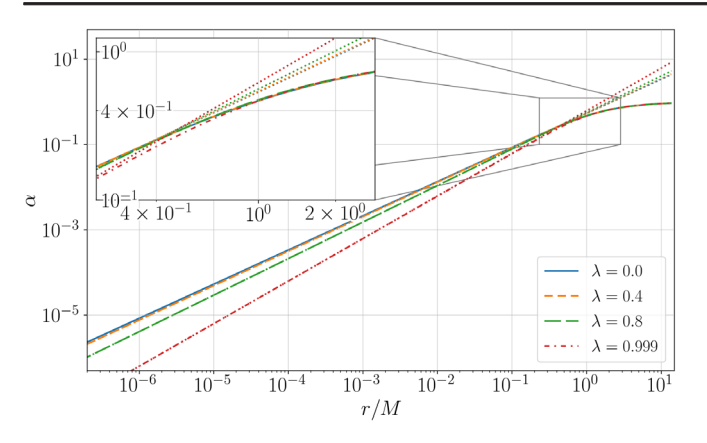


FIG. 10. The numerical profile of the lapse $\alpha(r)$ for $\lambda \in \{0, 0.4, 0.8, 0.999\}$ for zeroth-order shock-avoiding slices with $a_0 = 4/3$.

spacetimes. In addition to $1 + \log$ slicing we consider several other slicing conditions, specified by their corresponding Bona-Massó functions $f(\alpha)$, that have been adopted in numerical simulations. For some of these

conditions the slices can be constructed analytically, while for others we use numerical root-finding to solve rather unwieldy quartic equations. We identify critical parameters for these slices, parametrized by the charge-to-mass ratio $\lambda = Q/M$, and transform to isotropic coordinates as they would likely be adopted in numerical simulations. In particular we observe that, in the extremal limit $\lambda \to 1$, all slices approach a unique slice that is independent of the Bona-Massó functions considered in this paper, as we anticipate in Sec. III.

ACKNOWLEDGMENTS

S. E. L. acknowledges support through an undergraduate research fellowship at Bowdoin College, and H. P. O. would like to thank Bowdoin College and its Department of Physics and Astronomy for hospitality. This work was supported in part by National Science Foundation (NSF) Grant No. PHY-2010394 to Bowdoin College and the Coordenação de Aperfeiçoamento de Pessoal de Nível Superior—Brasil (CAPES)—Finance Code 001.

- [1] C. Bona, J. Massó, E. Seidel, and J. Stela, A New Formalism for Numerical Relativity, Phys. Rev. Lett. **75**, 600 (1995).
- [2] M. Alcubierre and B. Brügmann, Simple excision of a black hole in 3 + 1 numerical relativity, Phys. Rev. D **63**, 104006 (2001).
- [3] M. Alcubierre, B. Brügmann, P. Diener, M. Koppitz, D. Pollney, E. Seidel, and R. Takahashi, Gauge conditions for long-term numerical black hole evolutions without excision, Phys. Rev. D 67, 084023 (2003).
- [4] J. R. van Meter, J. G. Baker, M. Koppitz, and D.-I. Choi, How to move a black hole without excision: Gauge conditions for the numerical evolution of a moving puncture, Phys. Rev. D 73, 124011 (2006).
- [5] M. Campanelli, C. O. Lousto, P. Marronetti, and Y. Zlochower, Accurate Evolutions of Orbiting Black-Hole Binaries without Excision, Phys. Rev. Lett. 96, 111101 (2006).
- [6] J. G. Baker, J. Centrella, D.-I. Choi, M. Koppitz, and J. van Meter, Gravitational-Wave Extraction from an Inspiraling Configuration of Merging Black Holes, Phys. Rev. Lett. 96, 111102 (2006).
- [7] M. Hannam, S. Husa, D. Pollney, B. Brügmann, and N. Ó. Murchadha, Geometry and Regularity of Moving Punctures, Phys. Rev. Lett. 99, 241102 (2007).
- [8] M. Hannam, S. Husa, B. Brügmann, J. A. González, U. Sperhake, and N. Ó. Murchadha, Where do moving punctures go?, J. Phys. Conf. Ser. 66, 012047 (2007).
- [9] T. W. Baumgarte and S. G. Naculich, Analytical representation of a black hole puncture solution, Phys. Rev. D 75, 067502 (2007).

- [10] M. Hannam, S. Husa, F. Ohme, B. Brügmann, and N. Ó Murchadha, Wormholes and trumpets: Schwarzschild spacetime for the moving-puncture generation, Phys. Rev. D 78, 064020 (2008).
- [11] B. Brügmann, Schwarzschild black hole as moving puncture in isotropic coordinates, Gen. Relativ. Gravit. **41**, 2131 (2009).
- [12] M. Alcubierre, J. C. Degollado, and M. Salgado, Einstein-Maxwell system in 3+1 form and initial data for multiple charged black holes, Phys. Rev. D **80**, 104022 (2009).
- [13] M. Zilhao, V. Cardoso, C. Herdeiro, L. Lehner, and U. Sperhake, Collisions of charged black holes, Phys. Rev. D 85, 124062 (2012).
- [14] M. Zilhão, V. Cardoso, C. Herdeiro, L. Lehner, and U. Sperhake, Collisions of oppositely charged black holes, Phys. Rev. D 89, 044008 (2014).
- [15] M. Zilhão, V. Cardoso, C. Herdeiro, L. Lehner, and U. Sperhake, Head-on collisions of charged black holes from rest, Springer Proc. Math. Stat. 60, 451 (2014).
- [16] M. Zilhão, V. Cardoso, C. Herdeiro, L. Lehner, and U. Sperhake, Dynamics of charged black holes, in 13th Marcel Grossmann Meeting on Recent Developments in Theoretical and Experimental General Relativity, Astrophysics, and Relativistic Field Theories (World Scientific, Singapore, 2015), pp. 983–985.
- [17] P. Jai-akson, A. Chatrabhuti, O. Evnin, and L. Lehner, Black hole merger estimates in Einstein-Maxwell and Einstein-Maxwell-dilaton gravity, Phys. Rev. D 96, 044031 (2017).

- [18] G. Bozzola and V. Paschalidis, General Relativistic Simulations of the Quasicircular Inspiral and Merger of Charged Black Holes: GW150914 and Fundamental Physics Implications, Phys. Rev. Lett. 126, 041103 (2021).
- [19] G. Bozzola and V. Paschalidis, Numerical-relativity simulations of the quasicircular inspiral and merger of nonspinning, charged black holes: Methods and comparison with approximate approaches, Phys. Rev. D 104, 044004 (2021).
- [20] G. Bozzola, Does Charge Matter in High-Energy Collisions of Black Holes?, Phys. Rev. Lett. 128, 071101 (2022).
- [21] S. Mukherjee, N. K. Johnson-McDaniel, W. Tichy, and S. L. Liebling, Conformally curved initial data for charged, spinning black hole binaries on arbitrary orbits, arXiv: 2202.12133.
- [22] R. Luna, G. Bozzola, V. Cardoso, V. Paschalidis, and M. Zilhão, Kicks in charged black hole binaries, Phys. Rev. D 106, 084017 (2022).
- [23] T. W. Baumgarte and H. P. de Oliveira, Bona-Massó slicing conditions and the lapse close to black-hole punctures, Phys. Rev. D 105, 064045 (2022).
- [24] T. W. Baumgarte and S. L. Shapiro, *Numerical Relativity: Solving Einstein's Equations on the Computer* (Cambridge University Press, Cambridge, England, 2010).
- [25] B. Reimann and B. Brügmann, Maximal slicing for puncture evolutions of Schwarzschild and Reissner-Nordstrom black holes, Phys. Rev. D 69, 044006 (2004).
- [26] B. Reimann and B. Bruegmann, Late time analysis for maximal slicing of Reissner-Nordstrom puncture evolutions, Phys. Rev. D 69, 124009 (2004).

- [27] R. Panosso Macedo, J. L. Jaramillo, and M. Ansorg, Hyper-boloidal slicing approach to quasi-normal mode expansions: The Reissner-Nordström case, Phys. Rev. D 98, 124005 (2018).
- [28] M. Alcubierre, Appearance of coordinate shocks in hyperbolic formalisms of general relativity, Phys. Rev. D 55, 5981 (1997).
- [29] K. A. Dennison and T. W. Baumgarte, A simple family of analytical trumpet slices of the Schwarzschild spacetime, Classical Quantum Gravity 31, 117001 (2014).
- [30] K. A. Dennison, T. W. Baumgarte, and P. J. Montero, Trumpet Slices in Kerr Spacetimes, Phys. Rev. Lett. 113, 261101 (2014).
- [31] E. Jiménez-Vázquez and M. Alcubierre, Critical gravitational collapse of a non-minimally coupled scalar field, Phys. Rev. D 105, 064071 (2022).
- [32] T. W. Baumgarte and D. Hilditch, Shock-avoiding slicing conditions: Tests and calibrations, Phys. Rev. D 106, 044014 (2022).
- [33] M. Alcubierre, Hyperbolic slicings of spacetime: Singularity avoidance and gauge shocks, Classical Quantum Gravity 20, 607 (2003).
- [34] J. Healy, I. Ruchlin, C. O. Lousto, and Y. Zlochower, High energy collisions of black holes numerically revisited, Phys. Rev. D 94, 104020 (2016).
- [35] I. Ruchlin, J. Healy, C.O. Lousto, and Y. Zlochower, Puncture initial data for black-hole binaries with high spins and high boosts, Phys. Rev. D **95**, 024033 (2017).